Available online at www.sciencedirect.com
SCIENCE DIRECT
Fusion Engineering and Design 81 (2006) 2257–2265
Fusion Engineering and Design
www.elsevier.com/locate/fusengdes

Short communication

Power balance investigation in steady-state LHCD discharges on TRIAM-1M

K. Hanada [a,*], T. Sugata [b,1], M. Sakamoto [a], H. Zushi [a], K. Nakamura [a], K.N. Sato [a], H. Idei [a], M. Hasegawa [a], A. Higashijima [a], S. Kawasaki [a], H. Nakashima [a]

[a] *Research Institute for Applied Mechanics, Kyushu University, Fukuoka, Japan*
[b] *Interdisciplinary Graduate School of Engineering Sciences, Kyushu University, Japan*

Received 27 September 2005; received in revised form 15 February 2006; accepted 10 March 2006
Available online 21 June 2006

Abstract

A discharge longer than 5 h was successfully achieved on TRIAM-1M by fully non-inductive lower hybrid current drive (LHCD). The heat load distribution into the plasma facing components (PFCs) during the 5 h discharge was investigated using calorimetric measurements, which estimated that the injected radio frequency (RF) power coincided with the total heat load amount to the PFCs. The power balance, including the portion of direct loss power of the fast electrons and the heat flux due to the charge exchange (CX) process, was also investigated.

Keywords: Tokamak; Calorimetric measurement; Power balance; LHCD; Steady-state operation

1. Introduction

Steady-state operations are important for realizing a fusion power plant. In ITER, duration discharges greater than 1000 s are planned [1] and the estimated heat flux to the divertor is 5 MW/m^2 [2]. Treating this large, local heat flux is key for steady-state operations. One method to effectively treat heat is to cool the plasma facing components (PFCs). In Tore Supra, the CIEL project, which uses a toroidal pump limiter (TPL) experiment, has been enforced. The TPL is designed to extract power up to 15 MW [3] and the total heat extraction capability of Tore supra is upgraded to 25 MW for 1000 s [4]. Exhausting the huge heat load allows a high-power injected experiment to be implemented. In fact, an experiment with a discharge duration of more than 6 min and an injection power greater than 1 GJ, which means that an averaged heat load of 2.8 MW could be continuously removed, was successfully conducted [5]. Recently, a discharge greater than 1 h and a total injection power of 1.3 GJ were obtained on large helical

* Corresponding author. Tel.: +81 92 583 7706; fax: +81 92 573 6899.
E-mail address: hanada@triam.kyushu-u.ac.jp (K. Hanada).
[1] Present address: NTT advanced technology Ltd., Tokyo, Japan.

0920-3796/$ – see front matter © 2006 Elsevier B.V. All rights reserved.
doi:10.1016/j.fusengdes.2006.03.004

device (LHD) [6,7]. In both cases, the injected power of the devices (the lower hybrid wave (LHW) in Tore Supra, and the ion cyclotron range of frequency (ICRF), the electron cyclotron range of frequency (ECRF), and the neutral beam injection (NBI) in LHD) might be balanced to the power removed by the cooling system of the device. The cooling capability strongly depends on the distribution of the heat load to the PFCs, which is closely related to the power balance of the plasma. The radiative power emitted from a plasma will completely deposit on the first wall and the diffusion power will mainly deposit on the divertor plate around the divertor legs. This heat load distribution is noted in the ITER design report and a radiative power fraction of ≈75% is required [8]. Therefore, to achieve steady-state operations, it is important to investigate the power balance.

A discharge in excess of 5 h was maintained on TRIAM-1M by a lower hybrid current drive (LHCD) in a very low power region. This ultra long duration discharge is suitable for measuring the heat load since the temperature of the cooling water for the PFCs is saturated during the discharge. In this situation, the heat load can be derived from the steady temperature rise, which is shown in Section 3. The accuracy of the estimated heat load becomes better than that in short pulse discharges. Herein, the result of heat load to each PFC is described and the power balance of the discharge is shown. The experimental apparatus is introduced in Section 2, while Section 3 describes the heat load measurements. The experimental results are presented in Sections 4 and 5. Section 5 summarizes the conclusions.

2. Experimental apparatus

TRIAM-1M is a small size ($R_0 = 0.8$ m, $a \times b = 0.12\,\text{m} \times 0.18\,\text{m}$) tokamak with a high toroidal magnetic field up to 8 T excited by 16 toroidal field coils, which are composed of Nb_3Sn, a super-conducting material [9]. TRIAM-1M has two vacuum vessels. One is to avoid thermal penetration into the superconducting coils from the outside. The other is to keep a vacuum condition of 1×10^{-6} Pa or less since a low-pressure level ($<1 \times 10^{-5}$ Pa) must be maintained to make a plasma. Fig. 1 is a schematic toroidal cross section diagram of the latter vacuum vessel, which is made of stainless steel. The shaded area shows the region covered by the molybdenum divertor plates, which were installed on the bottom of the vacuum vessel.

Five limiters covered by molybdenum were installed on the vacuum vessel. Three poloidal ring limiters, which are referred to as "fixed limiters" in this paper and are shown in Fig. 1, were distributed in the toroidal direction to avoid direct contact of the plasma with the vacuum vessel. These limiters had toroidal widths of 32 mm, poloidal lengths of 1040 mm, and were 17 mm thick. They were installed on stainless steel bases,

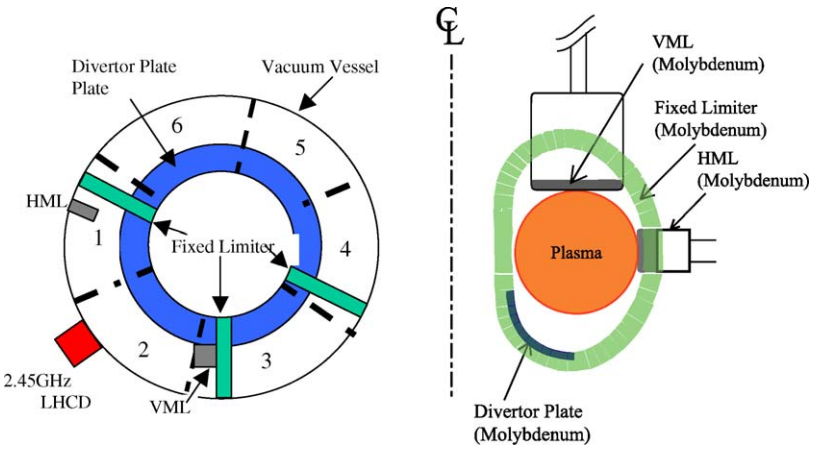

Fig. 1. (Right figure): Toroidal cross section diagram of the vacuum vessel for the plasma chamber. Numbering on the vacuum vessel indicates the branch of the cooling water channel. (Left figure): Schematically poloidal cross section diagram. The VML, the HML, fixed limiters, and divertor plate are illustrated on the same figure.

which played a role in attaching the fixed limiter to the surface of the vacuum vessel. These limiters could be indirectly cooled through water channels, which consisted of copper brazed on the stainless steel base. Since the inner and outer parts of the limiters could not equip water-cooling channels, the thermal transport of the inner and outer parts was quite poor compared to the other parts of the fixed limiters. A limiter installed on the top port of the vacuum vessel moved in the vertical direction. Hence, it is called the vertical movable limiter (VML). The limiter head was composed of molybdenum brazed on the water-cooled support, which was made of stainless steel using a thin copper foil attachment. Consequently, the thermal transport was significantly better than the other limiters. The moving distance could be varied between +32.5 and +80.0 mm using a bellows seal and a motor (the plus sign indicates that the direction is to the plasma side from the surface of the poloidal fixed limiter). The area of the limiter surface that faced the plasma was 30 mm × 160 mm. The other movable limiter could shift its surface in the horizontal direction up to +23 mm. Hence, it is called the horizontal movable limiter (HML). A single probe was installed on the HML and the parameters of the SOL plasma were measured. The size of plasma facing surface had a toroidal width of 34 mm and a poloidal length of 74 mm. This limiter was copper covered with molybdenum. The molybdenum cover was fixed to the copper base by four screws. Thus, the thermal transport was not as good as the VML. The copper base was attached to a water-cooled support.

Two types of microwave sources, which had frequencies of 2.45 and 8.2 GHz, were used to excite lower hybrid waves. In addition, a microwave source with a frequency of 170 GHz was used to inject electron cyclotron waves (ECW). All the microwave sources were installed as additional heating sources on TRIAM-1M. The microwave source with a frequency of 2.45 GHz could produce up to 50 kW in the steady state and was mainly used in the experiments described in this paper. The source microwave excited by a crystal oscillator of 2.45 GHz was amplified by a klystron. To inject microwaves into the plasma, high power microwaves were transferred through the waveguide with a rectangular cross section to a stainless steel launcher. The launching system was a 4 × 1 grill type waveguide array and the dimension of the grill waveguide was 15 mm × 71 mm. The phase difference, $\Delta\Phi$, between adjacent waveguides can be changed by a phase shifter. For the 5 h operation and the other long duration discharges, $\Delta\Phi = 110^\circ$ [10]. The injection power was estimated by the microwave power divided by the directional coupler in front of the launcher inlet. The monitored microwave power was measured with calibrated crystal diodes. Thus, the injected power can be measured during the discharge. To obtain the exact power absorbed into the plasma, the reflected power back to the launcher, the uncoupling power, and the power loss by propagation through the launcher need to be estimated. The reflected power back to the launcher was measured using the same method as that for the injected power. The reflected microwaves were mainly excited by coupling the microwaves with the plasma. The uncoupling microwave power was measured as the leaked microwave power through the vacuum window, which was made of sapphire. The power level was corrected using the following procedure. The microwave power leakage was measured at the window when a microwave was injected directly into the vacuum vessel without the plasma. The injected power was monitored as described above. Without the plasma present, all the injected RF power was absorbed by the wall, except for the leaked RF power through the window. The RF power flux to the wall was assumed to be homogeneous and the leaked power displayed a homogeneous RF power flux to the wall. The absolute RF power to the wall was estimated by comparing the leaked RF power to the injected RF power. The leaked power was measured in several short pulse discharges. Fig. 2 shows the results. Consequently, the estimated power leakage was as 7 W for every 1 kW of injection power. Unfor-

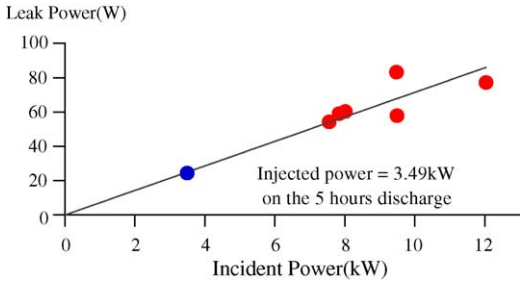

Fig. 2. Estimated RF power leakage as a function of incident RF power. Points in the range of 7–13 kW show the leaked power in long LHCD discharges with various injected power levels. The point around 3 kW shows the estimated data for the 5 h discharge since the data was not measured.

tunately, power leakage could not be measured during the 5 h discharge. The estimated value of the leaked power in the 5 h discharge was derived from the linear scaling shown in Fig. 2 and its power level (25 W) was insignificant in the total power balance.

The microwaves also lost power via a dumping process of microwave propagation in the waveguide. Since the launcher consists of stainless steel, the resistance on the surface of the waveguide was significant. The power loss on the launcher should be estimated to determine the net injected power and the measured value was obtained using the calorimetric method described below.

Fig. 3 illustrates the branch diagram of the cooling water system. The cooling water system for the HML is independent of the other cooling systems for the PFCs. The main cooling water system used pure water produced by the ion-exchange resin method. The branch of the cooling water for the 2.45 GHz microwave source is connected to the main cooling water loop through the heat exchanger shown in Fig. 3. The main cooling water channels were divided into 18 branches.

The cooling water temperature was measured at the points shown in Fig. 3 using thermistors with an accuracy of $\pm 0.02^{\circ}$. Thermistors are thermal sensitive resistors and their resistance values change significantly with a very small temperature change. The incremental changes in the water temperature between the inlet and outlet, ΔT, were necessary to estimate the heat load to each PFC. The data acquisition system was different from the main one since the water temperature must be continuously monitored until the PFCs were completely cooled after the discharge was terminated. Table 1 shows the flow rate of each PFC water branch.

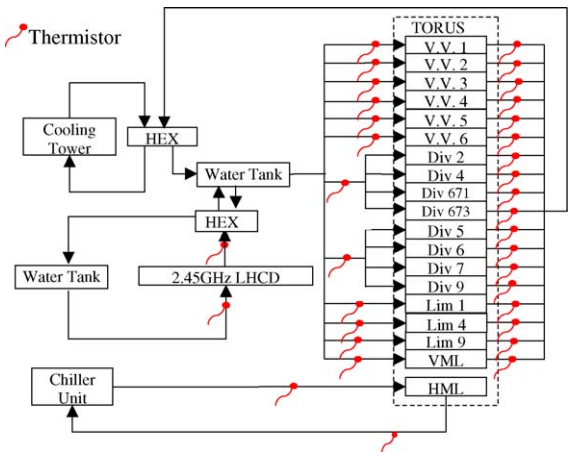

Fig. 3. Schematic diagram of the cooling water system. V.V. means the vacuum vessel for the plasma chamber, Div corresponds to the divertor plate, and Lim shows the fixed limiter shown in Fig. 1. HEX shows the heat exchanger.

Table 1
Flow rate of each PFC in the 5 h discharge

Vacuum vessel	Flow rate (g/s)	Divertor	Flow rate (g/s)	Limiter and LHCD	Flow rate (g/s)
No. 1	138	No. 2	60	No. 1 fixed limiter	74
No. 2	142	No. 4	71	No. 4 fixed limiter	65
No. 3	140	No. 5	63	No. 9 fixed limiter	43
No. 4	140	No. 6	68	VML	220
No. 5	137	No. 7	75	HML	217
No. 6	142	No. 9	72		
		No. 671	44	Launcher	367
		No. 673	62		

3. Estimation of the heat load from the incremental changes in water temperature

In this section, the estimated heat load from the incremental changes in the cooling water temperature is described. The following equation is used to calculate the heat load from water temperature,

$$Q = \frac{CG \int \Delta T \mathrm{d}t}{\tau_{\mathrm{dis}}}, \tag{1}$$

where Q is the heat load (W), C the specific heat of water (J/g K), G the flow rate of the cooling water (g/s), ΔT in the temperature difference (K), and τ_{dis} is the discharge duration (s). When the water temperature reaches the steady state, a simpler equation without integration is sufficient.

$$Q = CG\Delta T \tag{2}$$

Eq. (1) is used to measure the water temperature until the PFCs are completely cooled. Since a small temperature difference is difficult to measure, this method undervalues the results. When the cooling capability is poor, the small temperature difference will last. Thus, a large error appears in the results. In fact, it is difficult to measure the temperature difference until

the PFCs are completely cooled. On the other hand, the heat load can be accurately estimated when the water temperature is in the steady state.

When the water temperature of the inlet is varied, the temperature change of the PFCs due to the change in the cooling water temperature occurs. In this case, the PFCs work as a heat sink or source. The heat load estimated in this situation includes the heat caused by the temperature change of the PFCs, which leads to a large experimental error. Therefore, the heat load to the PFCs during the 5 h discharge was estimated by assuming that the inlet water temperature was also in the steady state.

4. Experimental results

Fig. 4 shows the waveforms of the plasma current, I_p, the net injected RF power, P_{LH}, and the intensity of the H_α signal during a 5 h discharge. The plasma current was fully driven by the LHW, except

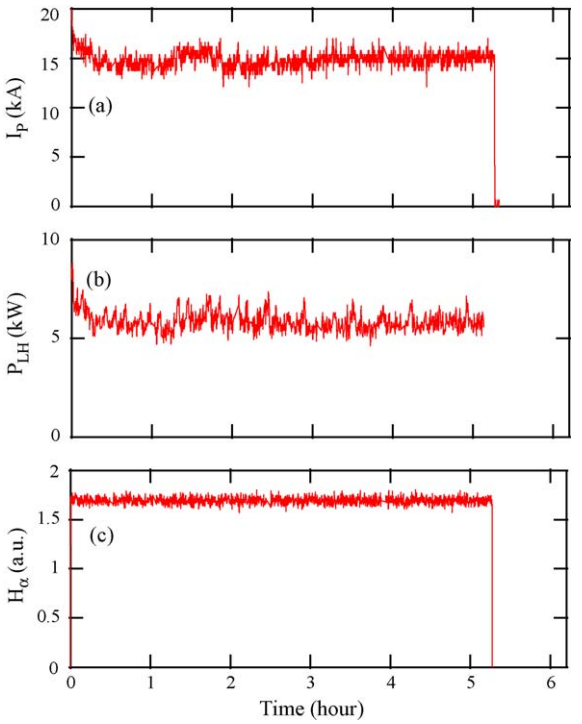

Fig. 4. Typical waveforms for a 5 h discharge. Plasma current (a), the net injected RF power detected by the crystal diodes (b), and the intensity of H_α signal (c) are plotted.

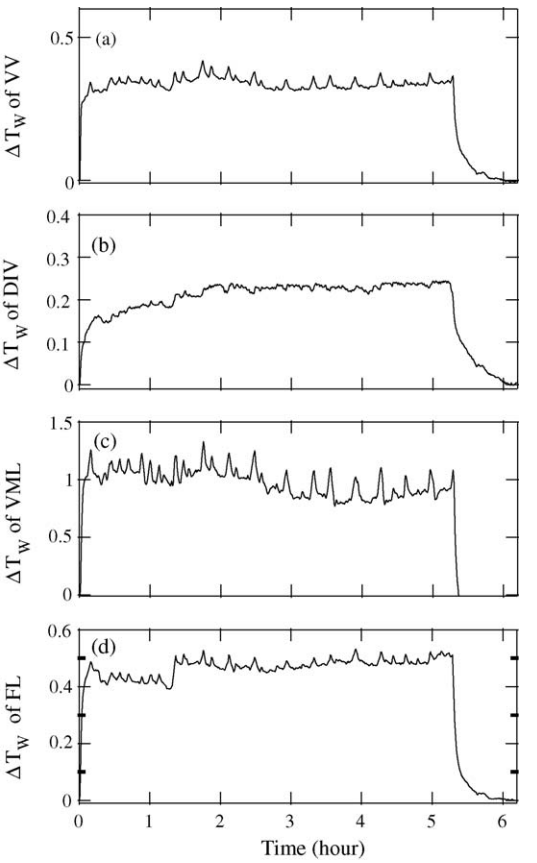

Fig. 5. Waveforms for the incremental changes in the water temperature of the vacuum vessel (a), the divertor plate (b), the vertical movable limiter (c), and the fixed limiter (d) are plotted. The vertical axis units in all figures are degrees.

at the beginning of the discharge (the first 0.2 s). The net injected RF power demonstrated the difference in power between the injected RF power monitored with the calibrated diode and the reflected one.

Fig. 5 shows typical waveforms for the incremental changes in the cooling water temperature for various PFCs. The slow fluctuation in the water temperature was caused by the changes in the coupling between the RF and the plasma. Details about this phenomenon are reported in Refs. [11,12]. In view of the stability of the inlet water temperature, calorimetric measurements were conducted around 4 h and all the parameters appear to be in the steady state. Hence, Eq. (2) is applicable. The VML was inserted into plasma to effectively remove the heat load. Thus, the last closed

flux surface (LCFS) was attached to the VML. The net injected power, which was measured by crystal diodes, was 5710 W and the calorimetric measurement of the launcher indicated that the estimated power loss at the launcher was 2220 W. The heat load of each PFC was estimated as follows. The 5 h discharge was on the limiter configuration at a given time and the divertor plate was far from the plasma. Therefore, the divertor plate only worked on a part of the vacuum vessel.

Fixed limiters	360 W (10%)
Movable limiters	1200 W (34%)
Vacuum vessel (include divertor plates)	1930 W (56%)

Two processes mainly caused the heat load to the limiters: (1) particle and heat fluxes diffusing from the core plasma to the LCFS and (2) fast electron heat fluxes via direct losses. The affect of radiation to the heat load of the limiters was neglected since the surface area of limiters was less than 2% of the total surface area in all PFCs. The heat flux to the limiters from the scrape-off layer (SOL) plasma was estimated from the electron temperature, T_e, and the density, n_e, measured with the probe installed on the HML. To measure the profiles of T_e and n_e, the HLM was inserted during several discharges, which were maintained by a LH power of 7200 W. The duration of these discharges was less than 10 s and the discharges were repeated using the same operation parameters. Fig. 6 shows the profiles of T_e and n_e in the SOL region during short pulse discharges. The head of the probe receded by 1 mm from the HML surface on the plasma side. Despite the deep insertion of the HML into the plasma, the value of T_e and n_e did not change in the range of 5 and 7 mm. This indicates that the head of the HML attaches to the LCFS. Thus, this method can determine the position of the LCFS. The dotted curves in Fig. 6 show the fitted profiles of the electron density and temperature. Unfortunately, the plasma parameters in the SOL region were not measured during the 5 h discharge since the probe position cannot be changed during the discharge and it is difficult to avoid the damage to the probe. The heat flux from the SOL plasma was derived from the plasma parameters as described in Refs. [13,14].

Next a 240 s discharge with a net injected power of 4400 W was executed to measure the direct loss power

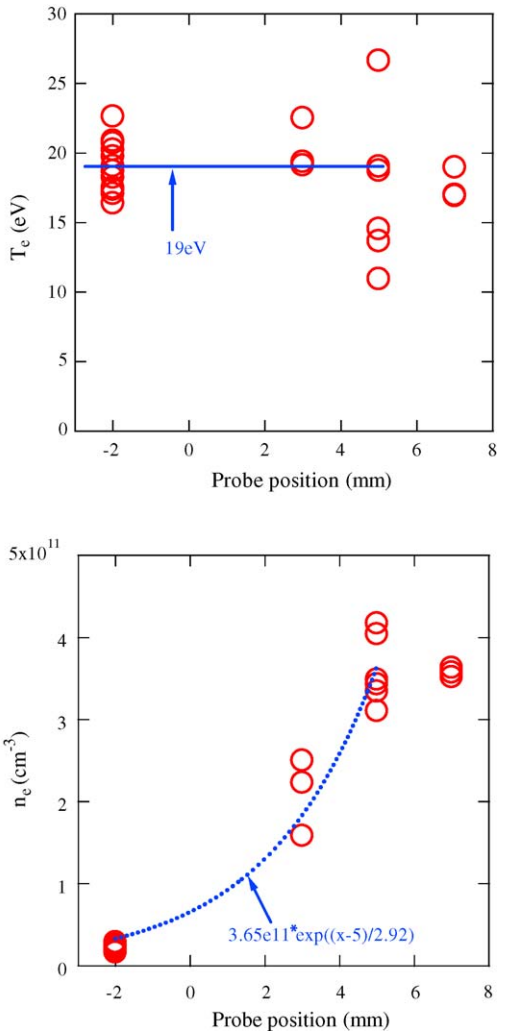

Fig. 6. Density and temperature profiles in the SOL plasma region.

of the fast electrons. The fast electrons, which were accelerated by microwaves, slowed via a collision process. Some of the fast electrons were occasionally scattered by magnetic fluctuations. The fast electrons quickly diffuse to the LCFS. The flux surface caused the orbits of the fast electrons to deviate. When the HML is attached to the LCFS, all of the fast electrons outside the LCFS collided with the HML and VML. Consequently, the power transferred by the direct loss of the fast electrons was measured as the heat load on the HML and VML. The total heat load to the HML and VML also included heat and particle fluxes from

the SOL plasma. Therefore, the heat load from the SOL plasma must be subtracted from the total heat load to the HML in order to estimate the fast electron direct loss [15]. Since both the VML and HML were inserted in this discharge, the fast electrons attacked both the VML and HML. The heat load to the VML and HML, which included the heat load from the SOL plasma and the fast electrons, was 590 and 260 W, respectively. The estimated value of heat load to the VML and HML from the SOL plasma was calculated as 430 and 160 W, respectively. Consequently, the estimated direct loss power of the fast electrons was 260 W during the 240 s discharge. The heat load to the other fixed limiter was mainly due to the SOL plasma and was 1100 W. The total heat load from the SOL plasma corresponded to 1690 W.

Only the VML was inserted into the plasma during the 5 h discharge. The injected RF power was 3490 W. It was assumed that the heat load from the SOL plasma was proportional to the net injected RF power, which is reasonable as shown in Ref. [13]. Under this assumption, the heat load from the SOL plasma was estimated as 1340 W. Hence, the fast electron power was estimated as 220 W for the 5 h discharge.

The heat load to the vacuum vessel was due to the following processes: (1) radiation, (2) charge exchange (CX), and (3) particle and heat fluxes from the SOL region. Radiation mainly affected the load of vacuum vessel since radiation was isotropic and vacuum vessel had the PFC most area. CX was comparable to radiation, but CX was anisotropic since the abundant neutral particles were anisotropic.

CX, which is a phenomenon between a charged particle and neutral particle, was anisotropic due to the uneven sources of neutral particles (in this experiment, mainly hydrogen atoms). Since the plasma parameters had toroidal symmetry, the toroidal asymmetry of a hydrogen atom was measured with the toroidal distribution of the H_α signal [16]. Fig. 7 shows the toroidal distribution of the H_α intensity in 5 h discharge. The particle source was on the VML due to the strong contact with the plasma. Fig. 8 shows the water temperature measurements on various parts of the vacuum vessel. The results for the No. 1 vacuum vessel were consistent with those for No. 4, but the results for Nos. 3 and 6 clearly differ. Nos. 1 and 4 each included a fixed limiter as shown in Fig. 1. On the other hand, No. 3 had a VML and a fixed limiter, while No. 6 did not have a limiter. Therefore, it is conceivable that the differing results are due to the CX effect. The estimated heat load difference between Nos. 3 and 6 was 55 W. The toroidal asymmetric heat load of the CX process caused this difference. The toroidal distribution of H_α (Fig. 7) was integrated along the toroidal distance in the range of the Nos. 3 and 6 parts of the vacuum vessel. The length of the toroidal distance is shown in Fig. 1. The ratio of the integrated H_α in the entire vacuum vessel to the difference of that in Nos. 3 and 6 was 3.18, indicating that the total heat load from the CX process was $55\,\text{W} \times 3.18 = 175\,\text{W}$. Consequently, the total heat load

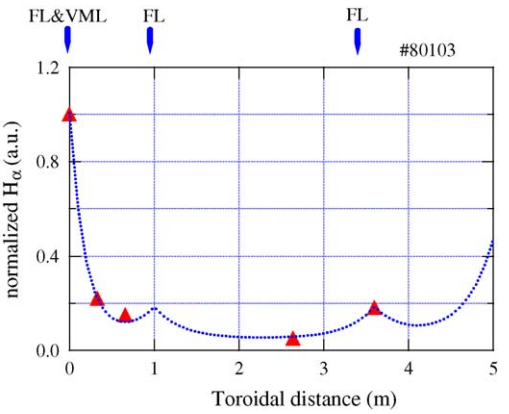

Fig. 7. Toroidal distribution of the H_α intensity along the toroidal distance, Z (m), at 18,000 s. The location of the VML in the toroidal direction corresponds to $Z = 0$ m of the abscissa axis. The vertical axis shows the H_α intensity normalized by that at the location of the VML. All circumference of the vacuum vessel corresponds to 5.28 m. The triangles are measured data and the dotted line shows the fitting data of the toroidal distribution. As described in Ref. [16], the particle sources in TRIAM-1M are three fixed limiters and VML. The toroidal distribution of the H_α intensity has the strong peaks at the fixed limiters and VML position and the observed FWHM value, λ, is 0.33 m in low density discharge [16]. The VML and one fixed limiter are installed at the position of 0 m in the figure. The next fixed limiter is installed at 1m and the final one is installed at 3.6 m. According to Ref. [16], the H_α intensity at 1 m and at 3.6 m are the same, therefore in this figure the peak values of the H_α intensity set to the same value in the fitting procedure. The value of FWHM is assumed as 0.33 m. As for the fitting around 0 m, two experimental data at $Z = 0$ and 0.4 m are used to do the fitting and as the result the value of λ is adjusted to 0.18 m. Finally, the distribution of the H_α intensity can be adjusted by $0.05 + 0.95(\exp(-|Z|/0.18) + \exp(-|5.28 - Z|/0.18)) + 0.13(\exp(-|1.0 - Z|/0.33) + \exp(-|3.6 - Z|/0.33))$ The offset value corresponds the recycling neutral from the vacuum vessel [16].

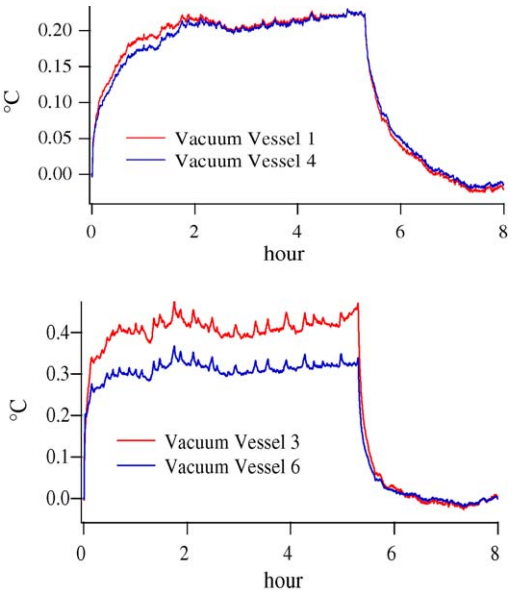

Fig. 8. Comparison of the vacuum vessel temperatures.

of the CX process was derived from the distribution of the H_α intensity and corresponds to 175 W during the 5 h discharge.

5. Power balance of a full LHCD 5 h discharge and conclusion

The power generated in a 2.45 GHz LHCD system (10260 W) is lost in the antenna (2220 W) and is reflected (4550 W). The remaining power (3490 W) is injected into the plasma and the virtual power couples with the fast electrons (3465 W). However, some power leaks (25 W) as microwave power. Most of the energy from the fast electrons is transferred to the thermal plasma via a slowing process (3205 W). The rest of the energy is inputted into the VML via a direct loss of fast electrons (220 W). The bulk plasma energy is distributed by three different processes: CX (175 W), radiation (1730 W), and diffusion (1340 W). The power balance of a long operation can be quantitatively estimated as shown in Fig. 9.

In this very low power steady-state discharge, the radiation power corresponds to 50% of the total power injected into the plasma. This appears to be caused by the high Z_{eff} due to the significantly low density.

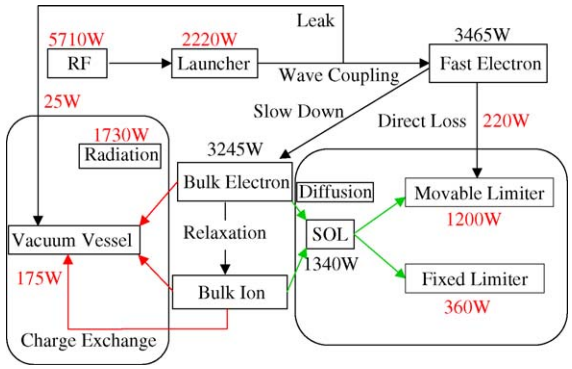

Fig. 9. Totally power balance of the 5 h discharge. The measured power is illustrated by characters. The net RF power is 5710 W. A part of the injected RF (2220 W) is lost in a launcher. The heat load to the vacuum vessel including divertor plate is composed of leaked RF (25 W), radiation (1730 W), charge exchange (175 W), and the total value is 1930 W. The radiation power (1730 W) is derived from total value of heat load to the vacuum vessel (1930 W)-CX (175 W)-leaked RF (25 W). The heat loads to the movable limiter and the fixed one are composed of direct loss of fast electron (220 W), diffusion of SOL plasma (1340 W) and the total value is 1560 W (to the movable limiter (1200 W) and to the fixed one (360 W)).

Acknowledgments

This work was partially performed under the framework of joint-use research at RIAM Kyushu University and the bi-directional collaboration organized by NIFS. This work is partially supported by a Grant-in-Aid for Scientific Research from Ministry of Education, Science, and Culture of Japan.

References

[1] Y. Shimomura, R. Aymar, V.A. Chuyanov, M. Huguet, H. Matsumoto, T. Mizoguchi, et al., Nucl. Fusion 41 (3) (2001) 309–316.
[2] ITER Physics Basis, Nucl. Fusion 39 (12) (1999) 2391–2469.
[3] J.-C. Vallet, M. Chantant, R. Mitteau, D. Thouvenin, J.J. Cordier, A. Ekedahl, et al., J. Nucl. Mater. 313–316 (2003) 706–710.
[4] J. Jacquinot, Nucl. Fusion 43 (12) (2003) 1583–1599.
[5] D. van Houtte, G. Martin, A. Becoulet, J. Bucalossi, G. Giruzzi, G.T. Hoang, et al., Nucl. Fusion 44 (5) (2004) L11–L15.
[6] T. Mutoh, R. Kumazawa, T. Seki, K. Saito, Y. Nakamura, S. Kubo, et al., J. Plasma Fusion Res. 81 (2005) 229–230.
[7] S. Kubo, Y. Yoshimura, T. Shimozuma, H. Igami, T. Notake, R. Kumazawa, et al., Proceedings AIP conference, vol. 787, 2005, pp. 411–414.
[8] D.J. Campbell, Phys. Plasmas 8 (5) (2001).

[9] S. Itoh, K.N. Sato, K. Nakamura, H. Zushi, M. Sakamoto, K. Hanada, et al., Nucl. Fusion 39 (1999) 1257.
[10] M. Sakamoto, S. Itoh, K.N. Sato, K. Nakamura, H. Zushi, K. Hanada, et al., Nucl. Fusion 40 (3Y) (2000) 453–460.
[11] H. Zushi, M. Sakamoto, K. Hanada, Y. Matsuo, K. Kuramoto, T. Sugata, et al., 12th International Congress of Plasma Physics, Nice France, P-1.082, 2004.
[12] H. Zushi, K. Nakamura, K. Hanada, K.N. Sato, M. Sakamoto, H. Idei, et al., 20th IAEA Fusion Energy Conference, Vilamoura, Portugal, OV/5-2, 2004.
[13] T. Maekawa, M. Nakamura, T. Komatsu, T. Kishino, Y. Kishigami, K. Makino, et al., Nucl. Fusion 32 (10) (1992).
[14] P.C. Stangeby, G.M. McCracken, Nucl. Fusion 30 (7) (1990).
[15] K. Hanada, Y. Shinoda, M. Sakamoto, S. Itoh, K. Nakamura, H. Zushi, et al., 29th EPS Plasma Physics and Controlled Fusion, P-2.085.
[16] M. Sakamoto, Y. Matsuo, H. Zushi, K. Nakamura, K. Hanada, K.N. Sato, et al., 20th IAEA Fusion Energy Conference, Vilamoura, Portugal, EX/P5-30, 2004.